Mathematical Formulation of the Tropospheric Delay Covariance for Very Long Baseline Interferometry Parameter Estimation

Robert Treuhaft*

ABSTRACT. — This report formulates the tropospheric covariance for Very Long Baseline Interferometry (VLBI) delay observations. The formulation describes calculations and data handling in COVTRP.f, the tropospheric covariance principal routine in MODEST, the Deep Space Network (DSN) VLBI parameter MODel-and-ESTimation software. The formulation in this report is intended to be an aid to anyone attempting to understand and/or modify the code. Two applications of the tropospheric covariance are identified: 1) It facilitates the calculation of the VLBI parameter-estimate covariance induced by tropospheric fluctuations, and 2) it also enables optimizing the parameter-estimate errors. It is shown that the formulation of the tropospheric covariance involves two-dimensional integrals over the structure function of refractivity (called D_χ). By casting the arguments of D_χ as quadratic forms and invoking a two-dimensional version of Gauss's theorem, the double integrals are reduced to single-dimension, line integrals, realizing an order of magnitude improvement in computation time. It is further argued that errors of $\approx$10% arise in this formulation of the tropospheric delay covariance, and in the COVTRP.f code, due to a flat-Earth assumption for intermediate-length ($\approx$500 km) baselines. Proposed simulations are described, which are aimed at evaluating use of the tropospheric covariance with various wind vectors and saturation scales, as well as the effects of Earth curvature.

*Tracking Systems and Applications Section.

The research described in this publication was carried out by the Jet Propulsion Laboratory, California Institute of Technology, under a contract with the National Aeronautics and Space Administration.

I. Introduction

The principal observation in Very Long Baseline Interferometry (VLBI) is the differential delay of extragalactic or spacecraft signals arriving at two Earth-fixed antennas [1]. The VLBI reference frame is derived by estimating parameters from the residual differential delays and, to a lesser extent, from the residual delay rates. Fluctuations in wet path–length refractivity, and therefore in path-length delay, are a principal error in VLBI parameter estimation [2]. The mathematical formulation of the tropospheric delay covariance is as calculated in COVTRP.f, a subroutine of MODEST, the VLBI parameter-estimation code. The calculated covariance is used to assess parameter errors due to wet tropospheric fluctuations. The covariance is also used to minimize parameter-estimate error by incorporating it into the estimation process. The tropospheric covariance was derived for long (> 500 km) baselines in Equation (13) of Treuhaft and Lanyi [2], referred to as TL13. The derivations in this report apply to very short baseline lengths and very long baseline lengths. Errors of $\approx$10% result in applying this formalism and/or code to intermediate baselines $\approx$500 km due to Earth curvature, as noted in the paragraph following Equation (13).

It is shown that, using quadratic forms and a modified version of Gauss's theorem, double integrals of the refractivity structure function in the covariance calculation can be converted to single integrals, reducing runtime by a factor of $\approx$10.

The following section shows how the tropospheric covariance can be used to evaluate VLBI parameter errors in the presence of tropospheric fluctuations. It also shows how the tropospheric covariance can be used in parameter estimation to derive optimal parameter estimates. Section III presents a derivation of the tropospheric covariance for any baseline vector in terms of double integrals of refractivity structure functions, which depend, in turn, on physical and geometric characteristics of the path delay (e.g., elevation and azimuth angles). As a prelude to transforming those double integrals into single integrals, Section IV casts the argument of the refractivity structure functions as a quadratic form, which is derived from the geometric and physical structure–function arguments of Section III. Section V describes a method for reducing those double integrals to single integrals. Section VI enumerates future studies to assess the use of the covariance.

II. Using the Tropospheric Covariance to Assess and Optimize Parameter-Estimate Performance

The next subsection shows how the parameter-estimate covariance arises from the tropospheric delay covariance for an arbitrary analysis mode. The parameter-estimate covariance is a means to assess the performance of estimated parameters. Subsection II.B shows how the tropospheric covariance can be used to optimize the analysis mode and thereby the performance of the parameter estimates.

A. Assessing Parameter-Estimate Performance by Applying the Tropospheric Covariance to the Calculation of Parameter-Estimate Covariance

A principal application of the tropospheric covariance is in the calculation of the parameter-estimate covariance due to tropospheric fluctuations. Below, in referring to a parameter estimate or observation, "residual" means the estimated or observed quantity minus a model value. In VLBI, residual parameter $\hat{P}_i$ could describe a baseline component or source coordinate or other geophysical or instrumental parameter. It is generally assumed that $\hat{P}_i$ is linearly related to the difference in residual propagation delays of the signals received at two stations, as in Equation (1) below. Let τ_{1k} be the k^{th} residual propagation delay, or pathlength, from the source of radio emission (natural-extragalactic object or spacecraft) to the receiver at station 1, and similarly for τ_{2k} at station 2. The VLBI observation (in the absence of error) is then $\tau_{1k} - \tau_{2k}$. The k index usually refers to epoch and/or observation geometry, including raypath incidence angle and azimuthal angle of the incident raypath with the baseline vector. Ignoring delay rates, the residual parameter estimate $\hat{P}_i$ is given by

$$\hat{P}_i = \sum_{k=1}^{n_{obs}} F_{ik}(\tau_{1k} - \tau_{2k}), \tag{1}$$

where n_{obs} is the number of $(\tau_{1k} - \tau_{2k})$ observations. The matrix F_{ik} is typically chosen to minimize the sum of squared differences between the parameter estimates and the true values of the parameters [3], i.e., to minimize $\sum_i \hat{P}_i^2$. But suboptimal F_{ik} are also frequently used because models needed for their calculation are imperfect or the runtime is too long.

The $(\tau_{1k} - \tau_{2k})$ observations are sensitive to tropospheric delays not common to stations 1 and 2. If the model for delays τ_{1k} and τ_{2k} were perfect except for contributions from tropospheric fluctuations, $\hat{P}_i$ would equal zero except for the fluctuating troposphere contribution. The covariance of $\hat{P}_i$ would depend on the covariance of observed delays $\tau_{1k} - \tau_{2k}$. In order to calculate the covariance of $\hat{P}_i$ due to troposheric delay fluctuations, note that the covariance of any two vectors x_i, x_j is

$$\mathrm{cov}\,(x_i, x_j) = \langle x_i x_j \rangle - \langle x_i \rangle \langle x_j \rangle, \tag{2}$$

where <> means ensemble average. For the troposphere, an ensemble is a set of refractivity patterns that can be modeled by Kolmogorov statistics [4]. The covariance

of $\hat{P}_i$ is therefore related to tropospheric delay covariances using Equations (1) and (2):

$$\begin{aligned}
\mathrm{cov}\left(\hat{P}_i, \hat{P}_j\right) =& \langle \hat{P}_i \hat{P}_j \rangle - \langle \hat{P}_i \rangle \langle \hat{P}_j \rangle \\
=& \sum_{k,l} F_{ik} F_{jl} \langle (\tau_{1k} - \tau_{2k})(\tau_{1l} - \tau_{2l}) \rangle - \sum_{k,l} F_{ik} F_{jl} \langle \tau_{1k} - \tau_{2k} \rangle \langle \tau_{1l} - \tau_{2l} \rangle \\
=& \sum_{k,l} F_{ik} F_{jl} \left(\langle \tau_{1k} \tau_{1l} \rangle - \langle \tau_{1k} \rangle \langle \tau_{1l} \rangle + \langle \tau_{2k} \tau_{2l} \rangle - \langle \tau_{2k} \rangle \langle \tau_{2l} \rangle \right) \\
& - \sum_{k,l} F_{ik} F_{jl} \left(\langle \tau_{1k} \tau_{2l} \rangle - \langle \tau_{1k} \rangle \langle \tau_{2l} \rangle + \langle \tau_{2k} \tau_{1l} \rangle - \langle \tau_{2k} \rangle \langle \tau_{1l} \rangle \right) \\
=& \sum_{k,l} F_{ik} F_{jl} \left(\mathrm{cov}\left(\tau_{1k}, \tau_{1l}\right) + \mathrm{cov}\left(\tau_{2k}, \tau_{2l}\right) - \mathrm{cov}\left(\tau_{1k}, \tau_{2l}\right) - \mathrm{cov}\left(\tau_{2k}, \tau_{1l}\right) \right)
\end{aligned} \tag{3}$$

It can be seen that calculation of the parameter covariance is enabled by tropospheric covariances, such as $\mathrm{cov}\left(\tau_{1k}, \tau_{1l}\right)$. The parameter covariance has variances on the diagonal and correlations in the off-diagonal terms and thus is a good indicator of the performance of residual parameter estimates. The sum of terms following $F_{ik}F_{jl}$ in the second and third lines of Equation (3), which is equivalent to the sum of terms after $F_{ik}F_{jl}$ in the last line of Equation (3), will be called the "troposphere observation covariance":

$$\mathrm{cov}\left(\tau_{1k} - \tau_{2k}, \tau_{1l} - \tau_{2l}\right) = \langle (\tau_{1k} - \tau_{2k})(\tau_{1l} - \tau_{2l}) \rangle - \langle \tau_{1k} - \tau_{2k} \rangle \langle \tau_{1l} - \tau_{2l} \rangle, \tag{4}$$

which will be used in the next subsection.

Throughout the rest of the report, "type 1" tropospheric covariances will be used to describe covariances like the first two to the right of the equal sign in the last line of Equation (3). These covariances are between delays at different times and raypaths but at the same station. "Type 2" tropospheric covariances are like those to the right of the minus sign in the last line of Equation (3), with covariances involving stations 1 and 2. Type 2 covariances, which describe station-to-station tropospheric correlations, were correctly ignored for long baselines in both TL13 and in MODEST, the Deep Space Network (DSN)–VLBI parameter-estimation algorithm. When stations are far apart, each delay in $\langle \tau_{1k} \tau_{2l} \rangle$ becomes independent of the other, and the type 2 terms in the last line of Equation (3) go to zero. Hence, for stations far apart,

$$\mathrm{cov}\left(\tau_{1k}, \tau_{2l}\right) = \langle \tau_{1k} \tau_{2l} \rangle - \langle \tau_{1k} \rangle \langle \tau_{2l} \rangle = \langle \tau_{1k} \rangle \langle \tau_{2l} \rangle - \langle \tau_{1k} \rangle \langle \tau_{2l} \rangle = 0. \tag{5}$$

However, $\mathrm{cov}\left(\tau_{1k}, \tau_{2l}\right)$ terms are included for the general covariance of this paper, expressed in Equation (17), where α and β can be any combination of 1 and 2. The type 2 terms, important for short baselines, are also included in the Fortran code of MODEST.

B. Optimizing Parameter-Estimate Performance by Applying the Tropospheric Covariance

The first application of the tropospheric covariance is to determine the parameter covariance given any F_{ik}'s. As mentioned above, suboptimal F_{ik}'s are sometimes used

for convenience. The second application of the tropospheric covariance is to find the optimal F_{ik}'s, $F_{ik_{opt}}$'s, which when inserted in Equation (1), produce optimal parameter residuals $\hat{P}_{i_{opt}}$ that minimize $\sum_i \hat{P}^2_{i_{opt}}$, as mentioned above. The $F_{ik_{opt}}{}'s$ can be gotten from the algorithm that calculates model delays, MODEST, using the troposphere observation covariance, as in Equation (4). Considering the observation residual delays to be = 0 except for tropospheric fluctuations, the optimal $F_{ik_{opt}}$ terms in Equation (1) can be calculated using the inverse of the troposphere observation covariance, W [3]:

$$F_{ik_{opt}} = \sum_{j=1}^{m_{param}} (A^T W A)^{-1}_{ij} (A^T W)_{jk}, \tag{6}$$

where A_{ij} is a matrix of partial derivatives of observation i with respect to parameter j, sometimes called the "design matrix" [5]. It is by using W that optimization of $F_{ik_{opt}}$, and thereby of $\hat{P}_{i_{opt}}$, takes place.

The rest of this report describes the calculation of tropospheric delay covariances, like those in the last line of Equation (3), in terms of observation geometry and epoch. It shows that tropospheric covariances are calculated with double integrals over refractivity structure functions and how those double integrals can be reduced to single integrals to save time.

III. Tropospheric Covariance in Terms of Refractivity-Structure-Function Integrals

The delay covariances at the bottom of Equation (3) above can be calculated by expressing delays like τ_{1k} in terms of refractivity along a raypath, $\vec{x}_1 + \vec{r}_1(\theta_{1k}, \phi_{1k}, z_1)$, as in Figure 1. For each station location, $\vec{x}_1$ in Figure 1, Earth's surface will be considered locally flat: a plane of a few tens of kilometers in extent, perpendicular to the Earth-radius vector (the local z-axis in Figure 1). In Figure 1, $\vec{r}_1(\theta_{1k}, \phi_{1k}, z_1)$ points from $\vec{x}_1$, at constant polar and azimuthal angles θ_{1k}, ϕ_{1k}, to a location in space at those angles, at an altitude z_1 above the tangent plane, which is the xy-plane in Figure 1, with y pointing into the plane of the paper. Ignoring bending, for time = 0, and the tropospheric refractivity at any arbitrary point $\vec{x}$ to be $\chi(\vec{x})$, a height increment dz_1 leads to a path increment $dz_1/\sin\theta_{1k}$, as in Figure 2. This path increment $dz_1/\sin\theta_{1k}$ in turn produces a path delay increment

$$d\tau_{1k}(\theta_{1k}, \phi_{1k}) = dz_1/\sin\theta_{1k} \chi(\vec{x}_1 + \vec{r}_1(\theta_{1k}, \phi_{1k}, z_1)),$$

as in the first line of Equation (7) below.

The delay τ_{1k} for insertion into terms like those at the bottom of Equation (3) is the integral of $d\tau_{1k}$:

$$\tau_{1k}(\theta_{1k}, \phi_{1k}, t_k) = \frac{1}{\sin\theta_{1k}} \int_0^h dz_1 \; \chi(\vec{x}_1 + \vec{r}_1(\theta_{1k}, \phi_{1k}, z_1) - \vec{v}_1 t_k), \tag{7}$$

where

$$\begin{aligned}\vec{r}_1(\theta_{1k}, \phi_{1k}, z_1) =& (r_1 \cos\theta_{1k} \cos\phi_{1k}, r_1 \cos\theta_{1k} \sin\phi_{1k}, r_1 \sin\theta_{1k}) \\ =& (z_1 \cot\theta_{1k} \cos\phi_{1k}, z_1 \cot\theta_{1k} \sin\phi_{1k}, z_1),\end{aligned}$$

and, with fixed θ_{1k} and ϕ_{1k}, the raypath for the k^{th} observation can be generated by stepping along values of $\vec{r}_1$ at values of z_1 above the tangent plane, ignoring bending.

In Equation (7), h is the wet tropospheric height, $\vec{v}_1$ is the wind velocity at station 1, and t_k is the time of the k^{th} observation, where it is understood that $\chi = \chi(\vec{x}_1 + \vec{r}_1(\theta_{1k}, \phi_{1k}, z_1))$ when $t_k = 0$.

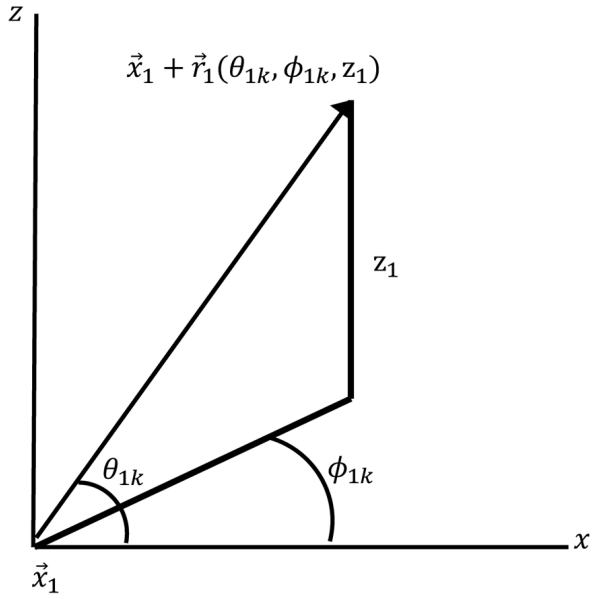

Figure 1. For a given height, z_1, above the (xy) tangent plane defined as perpendicular to the Earth-radius vector (the z-axis) at the station location ($\vec{x}_1$), the position at which refractivity is evaluated, at time = 0, is at $\vec{x}_1 + \vec{r}(\theta_{1k}, \phi_{1k}, z_1)$, for the k^{th} observation.

Inserting τ_{1k} and τ_{1l}, derived from the first line of Equation (7), in place of x_i and x_j in Equation (2) yields, for example, $cov(\tau_{1k}, \tau_{1l})$, a station-1, type-1 covariance:

$$\text{cov}\,(\tau_{1k}, \tau_{1l}) = \frac{1}{\sin\theta_{1k} \sin\theta_{1l}} \int_0^h \int_0^h dz_1 \; dz_1' \;\; [A - B] \tag{8}$$

where

$$\begin{aligned}A =& \langle \chi(\vec{x}_1 + \vec{r}_1(\theta_{1k}, \phi_{1k}, z_1) - \vec{v}_1 t_k) \chi(\vec{x}_1 + \vec{r}_1(\theta_{1l}, \phi_{1l}, z_1') - \vec{v}_1 t_l) \rangle \\ B =& \langle \chi(\vec{x}_1 + \vec{r}_1(\theta_{1k}, \phi_{1k}, z_1) - \vec{v}_1 t_k) \rangle \langle \chi(\vec{x}_1 + \vec{r}_1(\theta_{1l}, \phi_{1l}, z_1) - \vec{v}_1 t_l) \rangle.\end{aligned}$$

Assuming the mean square value of refractivity, $\langle \chi^2 \rangle$, does not vary with location in the troposphere (homogeneous assumption), TLA3 demonstrates that the

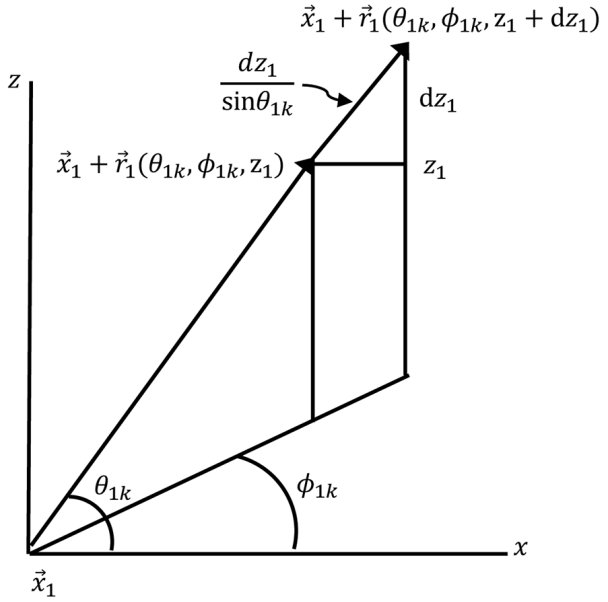

Figure 2. For a given height increment dz_1, the path increments by $dz_1/sin\theta_{1k}$, for the k^{th} observation.

ensemble-averaged product of refractivity at different locations $\vec{m}_1$ and $\vec{m}_2$ can be related to the refractivity structure function:

$$\langle \chi(\vec{m}_1)\chi(\vec{m}_2)\rangle = \langle \chi^2\rangle - \frac{1}{2}D_\chi(|\vec{m}_1 - \vec{m}_2|^2), \tag{9}$$

where the structure function, $D_\chi(|\vec{m}_1 - \vec{m}_2|^2) \equiv \langle(\chi(\vec{m}_1) - \chi(\vec{m}_2))^2\rangle$ and, from TL19, is given by

$$D_\chi(R) = \frac{C^2 R^{2/3}}{1 + (R/L)^{2/3}}, \tag{10}$$

with C being a normalization constant and L a saturation scale length, usually taken to be a few 1000 km. Using Equation (9) for the refractivity products in Equation (8), the covariance in Equation (8) becomes

$$\begin{aligned} \mathrm{cov}\,(\tau_{1k}, \tau_{1l}) =& \frac{1}{\sin\theta_{1k}\sin\theta_{1l}}\left[\langle\chi^2\rangle h^2 - \frac{1}{2}\int_0^h\int_0^h dz_1\ dz_1' D_\chi(|\vec{R}_{1kl}|^2) - \langle\chi\rangle^2 h^2\right] \\ =& \frac{1}{\sin\theta_{1k}\sin\theta_{1l}}\left[h^2\sigma_\chi^2 - \frac{1}{2}\int_0^h\int_0^h dz_1\ dz_1' D_\chi(|\vec{R}_{1kl}|^2)\right], \end{aligned} \tag{11}$$

where

$$\vec{R}_{1kl} = \vec{r}_1(\theta_{1k}, \phi_{1k}, z_1) - \vec{r}_1(\theta_{1l}, \phi_{1l}, z_1') - \vec{v}_1(t_k - t_l)$$

and $\sigma_\chi^2 \equiv \langle\chi^2\rangle - \langle\chi\rangle^2$ is assumed independent of the coordinates of the raypaths in Figures 1 or 2.

Putting $\vec{r}_1$ from the third line of Equation (7) into Equation (16):

$$\begin{aligned}|\vec{R}_{1kl}|^2 =&(z_1 \cot\theta_{1k}\cos\phi_{1k} - z_1' \cot\theta_{1l}\cos\phi_{1l} - v_1(t_k - t_l))^2 \\ &+ (z_1 \cot\theta_{1k}\sin\phi_{1k} - z_1' \cot\theta_{1l}\sin\phi_{1l})^2 \\ &+ (z_1 - z_1')^2,\end{aligned} \tag{12}$$

where the velocity of the wind is taken to lie along the x-axis.

The expression for the type 2 tropospheric covariance, $\mathrm{cov}\,(\tau_{1k}, \tau_{2l})$, needed for smaller baseline lengths, is derived by inserting τ_{2l} in place of x_j in Equation (2). The station 2 delay, τ_{2l}, is derived from the first line of Equation (7), with $1 \to 2$ and $k \to l$. The wind vector is taken to be the same at each station and along the x-axis, $\vec{v}_1 = \vec{v}_2 \equiv \vec{v} = (v_x, 0, 0)$:

$$\mathrm{cov}\,(\tau_{1k}, \tau_{2l}) = \frac{1}{\sin\theta_{1k}\sin\theta_{2l}}\left[h^2\sigma_\chi^2 - \frac{1}{2}\int_0^h \int_0^h dz_1\ dz_2' D_\chi(|\vec{R}_{12}|^2)\right] \tag{13}$$

where

$$\begin{aligned}|\vec{R}_{12}|^2 =&|(\vec{x}_1 + \vec{r}_1) - (\vec{x}_2 + \vec{r}_2) - \vec{v}(t_k - t_l)|^2 \\ =&B_x + z_1 \cot\theta_{1k}\cos\phi_{1k} - z_2' \cot\theta_{2l}\cos\phi_{2l} - v_x(t_k - t_l)^2 \\ &+ (z_1 \cot\theta_{1k}\sin\phi_{1k} - z_2' \cot\theta_{2l}\sin\phi_{2l})^2 \\ &+ (z_1 - z_2')^2\end{aligned}$$

where $\vec{B} \equiv \vec{x}_1 - \vec{x}_2$ is the baseline vector, and on the fourth line of Equation (13) is taken to lie along the x-axis with component B_x.

Note that the second line of Equation (13) assumes a very short baseline, by applying Equation (7) to get τ_{2l} for insertion into Equation (2). For short baselines or a flat Earth, the orientation of the tangent plane (or zenith) at each station is nearly identical to that at the other. For intermediate (≈500 km) baselines and a spherical Earth, the orientation of tangent planes, and therefore zenith directions, can be up to a few degrees different between stations. These differences can introduce errors into type 2 covariances treated as in Equation (13). For very long baselines > 1000 km, Equation (5) holds and $cov(\tau_{1k}, \tau_{2l}) = 0$ and errors due to large differences in tangent plane orientations do not matter. In future versions of the mathematical formulation of the covariance, and of the code, all z_2', θ_{2l}, and ϕ_{2l} coordinates must be transformed to the same coordinate system in which z_1, θ_{1k}, and ϕ_{1k} are expressed, before deriving expressions like Equation (13).

For now, the order of the error incurred in the code using the tropospheric covariance for intermediate baselines of ≈500 km is estimated to be about 10% (≈500 km/Earth Radius). A careful error analysis of the flat-Earth assumption in type 2 covariances as a function of baseline length will be investigated by simulations as suggested in Section VI. These simulations should prompt the transformations of coordinates to the

same reference frame, as mentioned above. It should also be noted that because current DSN baseline lengths are more than an Earth radius or less than 10 km, the "Earth-curvature" error will not have a big effect on the calculated tropospheric delay covariance, it is not treated in the code, and the formulation in this report will continue without modelling Earth curvature.

In the general case with the baseline vector $\vec{B} \equiv (B_x, B_y, B_z)$ and the wind velocity vector $\vec{v} = (v_x,\, v_y,\, v_z)$ (assumed the same at each station), Equation (13) becomes

$$\begin{aligned} cov(\tau_{1k}, \tau_{2l}) = & \frac{1}{\sin\theta_{1k} \sin\theta_{2l}} \Bigg[h^2 \sigma_\chi^2 - \frac{1}{2} \int_0^h \int_0^h dz_1 \; dz_2' D_\chi [(B_x - v_x(t_k - t_l) \\ & + z_1 \cot\theta_{1k} \cos\phi_{1k} - z_2' \cot\theta_{2l} \cos\phi_{2l})^2 \\ & + (B_y - v_y(t_k - t_l) + z_1 \cot\theta_{1k} \sin\phi_{1k} - z_2' \cot\theta_{2l} \sin\phi_{2l})^2 \\ & + (B_z - v_z(t_k - t_l) + z_1 - z_2')^2)] \Bigg]. \end{aligned} \tag{14}$$

Note that formally, a vertical z component of wind velocity is included, but lateral (x-y) wind vectors are most often considered.

The following, more general expression for the tropospheric covariance can be applied to produce type 1 and type 2 covariances. It is derived by letting the station indices in Equation (14) be general, and it facilitates comparison with the code:

$$\begin{aligned} cov(\tau_{\alpha,k}, \tau_{\beta,l}) = & \frac{1}{\sin\theta_{\alpha,k} \sin\theta_{\beta,l}} \Bigg[h^2 \sigma_\chi^2 - \frac{1}{2} \int_0^h \int_0^h dz_\alpha \; dz_\beta' D_\chi [(B_x - v_x(t_k - t_l) \\ & + z_\alpha \cot\theta_{\alpha,k} \cos\phi_{\alpha,k} - z_\beta' \cot\theta_{\beta,l} \cos\phi_{\beta,l})^2 \\ & + (B_y - v_y(t_k - t_l) + z_\alpha \cot\theta_{\alpha,k} \sin\phi_{\alpha,k} - z_\beta' \cot\theta_{\beta,l} \sin\phi_{\beta,l})^2 \\ & + (B_z - v_z(t_k - t_l) + z_\alpha - z_\beta')^2)] \Bigg], \end{aligned} \tag{15}$$

where α and β are the station indices and take on the values of 1 or 2. Written explicitly, z_α and z_β' are the z-coordinates of the raypaths above station α and station β, respectively. Note that the first two terms in the argument of D_χ, for each component of $\vec{B}$ and $\vec{v}$, do not depend on the geometric properties of the raypaths, neither the angular coordinates of the observation, nor the z_α or z_β' coordinates of the first or second raypath in the covariance calculation. These terms simply depend on ground-based differential descriptors such as baseline vector and differential observation epoch. For this reason, and to better understand the code, the vector $\vec{\rho}_0$ is defined as

$$\vec{\rho}_0 \equiv \vec{B} - \vec{v}_\alpha t_k + \vec{v}_\beta t_l, \tag{16}$$

where the velocity vector is allowed to be different at stations α and β. With

Equation (16), Equation (15) becomes

$$
\begin{aligned}
cov(\tau_{\alpha,k},\tau_{\beta,l}) =& \frac{1}{\sin\theta_{\alpha,k}\sin\theta_{\beta,l}}\Bigg[h^2\sigma_\chi^2 - \frac{1}{2}\int_0^h\int_0^h dz_\alpha\ dz'_\beta D_\chi[(\rho_{0x} \\
&+ z_\alpha\cot\theta_{\alpha,k}\cos\phi_{\alpha,k} - z'_\beta\cot\theta_{\beta,l}\cos\phi_{\beta,l})^2 \\
&+ (\rho_{0y} + z_\alpha\cot\theta_{\alpha,k}\sin\phi_{\alpha,k} - z'_\beta\cot\theta_{\beta,l}\sin\phi_{\beta,l})^2 \\
&+ (\rho_{0z} + z_\alpha - z'_\beta)^2]\Bigg] \\
=& \frac{1}{\sin\theta_{\alpha,k}\sin\theta_{\beta,l}}\Bigg\{h^2\sigma_\chi^2 - \frac{1}{2}\int_0^h\int_0^h dz_\alpha\ dz'_\beta D_\chi\Bigg[\rho_0^2 \\
&+ \frac{z_\alpha^2}{\sin^2\theta_{\alpha k}} + \frac{z_\beta^{'2}}{\sin^2\theta_{\beta l}} + \frac{2z_\alpha\vec{\rho}_0\cdot\hat{e}_{\alpha k}}{\sin\theta_{\alpha k}} - \frac{2z'_\beta\vec{\rho}_0\cdot\hat{e}_{\beta l}}{\sin\theta_{\beta l}} - \frac{2z_\alpha z'_\beta\hat{e}_{\alpha k}\cdot\hat{e}_{\beta l}}{\sin\theta_{\alpha k}\sin\theta_{\beta l}}\Bigg]\Bigg\}
\end{aligned}
\tag{17}
$$

$$
\begin{aligned}
\text{where } \hat{e}_{\alpha k} &\equiv (\cos\theta_{\alpha k}\cos\phi_{1k}, \cos\theta_{\alpha k}\sin\phi_{\alpha k}, \sin\theta_{\alpha k}) \\
\hat{e}_{\beta l} &\equiv (\cos\theta_{\beta l}\cos\phi_{\beta l}, \cos\theta_{\beta l}\sin\phi_{\beta l}, \sin\theta_{\beta l})
\end{aligned}
$$

IV. Arguments of the Refractivity Structure Functions as Quadratic Forms

The process of reducing the double integral of Equation (17) to a single integral involves finding a function that has a divergence equal to D_χ. Finding this function as a simple integral of D_χ, as in Equation (35), is facilitated by expressing the argument of D_χ in Equation (17) as a quadratic form, $Q(x,y)$, with $x \equiv z_\alpha$ and $y \equiv z'_\beta$. Q is equated to the argument of D_χ in Equation (17) as

$$
\begin{aligned}
Q(x,y) &\equiv \rho_0^2 + \frac{x^2}{\sin^2\theta_{\alpha k}} + \frac{y^2}{\sin^2\theta_{\beta l}} + \frac{2x\vec{\rho}_0\cdot\hat{e}_{\alpha k}}{\sin\theta_{\alpha k}} - \frac{2y\vec{\rho}_0\cdot\hat{e}_{\beta l}}{\sin\theta_{\beta l}} - \frac{2xy\hat{e}_{\alpha k}\cdot\hat{e}_{\beta l}}{\sin\theta_{\alpha k}\sin\theta_{\beta l}} \\
&= \rho_0^2 + \frac{x^2}{\sin^2\theta_{\alpha k}} + \frac{y^2}{\sin^2\theta_{\beta l}} + 2\vec{b}\cdot\vec{x} - \frac{2xy\hat{e}_{\alpha k}\cdot\hat{e}_{\beta l}}{\sin\theta_{\alpha k}\sin\theta_{\beta l}},
\end{aligned}
\tag{18}
$$

where

$$
\vec{x} \equiv \begin{bmatrix} x \\ y \end{bmatrix} \text{ and } \vec{b} \equiv \begin{bmatrix} b_x \\ b_y \end{bmatrix} \equiv \begin{bmatrix} \frac{\hat{e}_{\alpha k}\cdot\vec{\rho}_0}{\sin\theta_{\alpha k}} \\ \\ \frac{-\hat{e}_{\beta l}\cdot\vec{\rho}_0}{\sin\theta_{\beta_l}}. \end{bmatrix}
$$

Q is further equated to the general expression for a quadratic form as

$$
\begin{aligned}
Q &= (\vec{x}-\vec{\mu})^T\Gamma(\vec{x}-\vec{\mu}) + Q_0 \\
&= \begin{bmatrix}(x-\mu_x) & (y-\mu_y)\end{bmatrix}\begin{bmatrix}\Gamma_{11} & \Gamma_{12} \\ \Gamma_{21} & \Gamma_{22}\end{bmatrix}\begin{bmatrix}x-\mu_x \\ y-\mu_y\end{bmatrix} + Q_0
\end{aligned}
\tag{19}
$$

and we want to find Γ, μ_x, μ_y, and Q_0 that make Equation (19) equivalent to Equation (18). It will be seen that derivatives of Q with respect to x and y as in

Equation (19) are simple and needed to convert the double integrals of Equation (17) to single integrals.

In order to find the matrix Γ, the vector $\vec{\mu}$, and the scalar Q_0, which make Equation (19) account for all the terms in Equation (18), expand the right side of Equation (19) as

$$\begin{aligned} Q &= \Gamma_{11}x^2 - 2\Gamma_{11}\mu_x x + \Gamma_{11}\mu_x^2 + \Gamma_{12}xy - \Gamma_{12}\mu_y x + \Gamma_{12}\mu_x\mu_y - \Gamma_{12}y\mu_x \\ &+ \Gamma_{21}yx + \Gamma_{21}\mu_x\mu_y - \Gamma_{21}x\mu_y - \Gamma_{21}y\mu_x + \Gamma_{22}y^2 - 2\Gamma_{22}\mu_y y + \Gamma_{22}\mu_y^2 + Q_0. \end{aligned} \quad (20)$$

In Equations (21), (22), and (23), Γ, μ, and Q_0 in Equation (20) are specified in terms of the physical arguments of D_χ in Equation (18). In order to find Γ, note like terms in Equations (20) and (18), and equate their coefficients. For example, the coefficient of x^2 in Equation (18) is $1/\sin^2\theta_{\alpha k}$, and in Equation (20) the coefficient of x^2 is Γ_{11}. Therefore, equating coefficients of x^2, y^2, and xy in Equations (18) and (20) yields

$$\Gamma_{11} = \frac{1}{\sin^2\theta_{\alpha k}} \qquad \Gamma_{22} = \frac{1}{\sin^2\theta_{\beta l}} \quad \Gamma_{12} = \Gamma_{21} = \frac{-\hat{e}_{\alpha k}\cdot\hat{e}_{\beta l}}{\sin\theta_{\alpha k}\sin\theta_{\beta l}}. \quad (21)$$

Noting that $\vec{b}\cdot\vec{x} = b_x x + b_y y$ and equating the coefficients of x and y in Equations (18) and (20) yields

$$\begin{aligned} 2b_x &= -2\Gamma_{11}\mu_x - \Gamma_{12}\mu_y - \Gamma_{21}\mu_y = -2\Gamma_{11}\mu_x - 2\Gamma_{12}\mu_y \\ 2b_y &= -2\Gamma_{12}\mu_x - 2\Gamma_{22}\mu_y \\ &\Longrightarrow \quad \vec{b} = -\Gamma\vec{\mu} \text{ or } \vec{\mu} = -\Gamma^{-1}\vec{b}. \end{aligned} \quad (22)$$

Note that Equation (22) shows that the $\vec{\mu}$ term is needed in the quadratic form because of the $\vec{b}$ term in Equation (18), which is, in turn, needed because of the linear $\vec{x}$ term in Equation (18).

Having specified Γ and μ in terms of the physical expression for Q in Equation (18), Q_0 is specified by equating Equations (18) and (20) after setting x and $y = 0$ in both equations:

$$\begin{aligned} \rho_0^2 &= \Gamma_{11}\mu_x^2 + \Gamma_{12}\mu_x\mu_y + \Gamma_{21}\mu_x\mu_y + \Gamma_{22}\mu_y^2 + Q_0 \\ Q_0 &= \rho_0^2 - \vec{\mu}^T\Gamma\vec{\mu} \;=\; \rho_0^2 - \vec{b}^T\Gamma^{-1}\vec{b}. \end{aligned} \quad (23)$$

Table 1 summarizes Equations (21), (22), and (23), expressing quadratic form quantities in terms of geometric quantities of Equations (17) and (18) in the argument of the refractivity structure function, D_χ.

V. Transforming the 2D Refractivity Integral to 1D

This section derives the transformation from a 2-D integral like that in Equation (17) to a 1D integral, as outlined by an informal memo by Mark Finger in 1988 [7].

Table 1. Summary of Equations (21), (22), and (23).

(21)	$\Gamma = \begin{bmatrix} \frac{1}{\sin^2\theta_{\alpha k}} & \frac{-\hat{e}_{\alpha k}\cdot\hat{e}_{\beta l}}{\sin\theta_{\alpha k}\sin\theta_{\beta l}} \\ \frac{-\hat{e}_{\alpha k}\cdot\hat{e}_{\beta l}}{\sin\theta_{\alpha k}\sin\theta_{\beta l}} & \frac{1}{\sin^2\theta_{\beta l}} \end{bmatrix}$
(22)	$\vec{\mu} = -\Gamma^{-1}\vec{b}$
(23)	$Q_0 = \rho_0^2 - \vec{b}^T\Gamma^{-1}\vec{b}$

A. From 2D Integral to 1D for a General Function $\vec{f}$

This treatment, which fills in the details of MF88, starts by rewriting the argument of the refractivity structure function in the integral in Equation (17) in terms of Q as in Equation (19):

$$\text{Integral} \;=\; \int_0^h \int_0^h D_\chi(Q(x,y))dxdy \tag{24}$$

The method for demonstrating the general 2D to 1D integral is based on Gauss's theorem for transforming 3D to 2D integrals [6]. The demonstration of that transformation starts with an infinitesimal, rectangular volume, with normals pointing outward from each surface. But instead of a 3D infinitesimal volume, we start with a 2D infinitesimal surface, with rectangular sides of length Δx and Δy, and calculate the dot product of an arbitrary vector function $\vec{f}$, with outward normals to each linear segment of the rectangle, and their derivatives. The dot product is then multiplied by the length of the corresponding linear segment. Ultimately, we want to show that the sum of those dot-product expressions over the four lines of the rectangle in Figure 3 is equal to the divergence of the function times the infinitesimal area of the surface.

Figure 3 shows rectangle i, with midpoints of sides one through four, $\vec{P}_{i,1-4}$, and corner reference point $\vec{P}_{i_0}$.

The dot-product expressions of $\vec{f}(\vec{P}_{i,j})\cdot\hat{n}_{i,j}d\psi_{i,j}$ are summed over the four sides of rectangle i:

$$\text{Infinitesimal linear sum of dot products at } \vec{P}_{i,0} \;=\; \sum_{j=1,4} \hat{n}_{i,j}\cdot\vec{f}(\vec{P}_{i,j})d\psi_{i,j}, \tag{25}$$

where $d\psi_{i,j}$ is a positive pathlength on the j^{th} side of rectangle$_i$, with value either Δx or Δy (independent of i). The side $j=1$ term of the sum in Equation (25), with $\hat{n}_{i,1} = -\hat{x}$, is therefore:

$$\begin{aligned} -\hat{x}\cdot\vec{f}\left(x, y+\frac{\Delta y}{2}\right)\Delta y &= -\,\hat{x}\cdot\left[\vec{f}(x,y) + \frac{d\vec{f}(\vec{P}_{i,0})}{dy}\frac{\Delta y}{2}\right]\Delta y \\ &\equiv \left[-f_x(\vec{P}_{i,0}) - \frac{df_x(\vec{P}_{i,0})}{dy}\frac{\Delta y}{2}\right]\Delta y. \end{aligned} \tag{26}$$

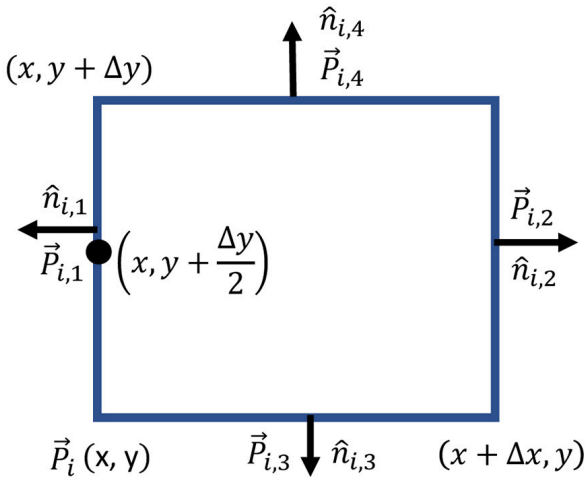

Figure 3. The i^{th} infinitesimal rectangle, with origin (corner) at $\vec{P}_{i,0}$. This rectangle, with side lengths of Δx and Δy, both positive, is the path along which the sum in Equation (25) is taken of the function $\vec{f}$ dotted into the normals shown. This sum is shown below to be equal to the two-dimensional divergence of $\vec{f}$, multiplied by the infinitesimal area $\Delta x \Delta y$.

In a similar way, suppressing the "$\vec{P}_{i,0}$" term and ignoring second-order derivatives like $\frac{d^2 f_x}{dxdy}$, side $j = 2$ of the sum is

$$\left[f_x + \frac{df_x}{dy}\frac{\Delta y}{2} + \frac{df_x}{dx}\Delta x \right] \Delta y, \tag{27}$$

side $j = 3$ of the sum is

$$\left[-f_y - \frac{df_y}{dx}\frac{\Delta x}{2} \right] \Delta x, \tag{28}$$

and side $j = 4$ of the sum is

$$\left[f_y + \frac{df_y}{dx}\frac{\Delta x}{2} + \frac{df_y}{dy}\Delta y \right] \Delta x. \tag{29}$$

Adding Equations (26) through (29) shows that infinitesimal linear sum i with corner $\vec{P}_{i,0}$ is

$$\sum_{j=1,4} \hat{n}_{i,j} \cdot \vec{f}(\vec{P}_{i,j}) d\psi_{i,j} = \left[\frac{df_x}{dx} + \frac{df_y}{dy} \right] \Delta x \Delta y \equiv \vec{\nabla}_2 \cdot \vec{f}(\vec{P}_{i,0}) dx dy, \tag{30}$$

where $\vec{\nabla}_2$ is the two-dimensional divergence defined by Equation (30), and $dxdy = \lim \Delta x \Delta y$ as they both tend toward zero.

In order to demonstrate that the double integral in Equation (24) can be expressed as four single-dimensional integrals, Equation (31) starts with Equation (24) and uses Equation (30) to sum infinitesimal rectangles, indexed by i, on both sides of Equation (30).

$$\int\int \vec{\nabla}_2 \cdot \vec{f}\, dxdy = \quad \sum_i \vec{\nabla}_2 \cdot \vec{f}(\vec{P}_{i,0}) dx dy = \sum_i \sum_{j=1}^{4} \hat{n}_{i,j}(\vec{P}_{i,j}) \cdot \vec{f}(\vec{P}_{i,j}) d\psi_{i,j}$$

$$= \sum_{j=1}^{4} \sum_i \hat{n}_{i,j}(\vec{P}_{i,j}) \quad \cdot \vec{f}(\vec{P}_{i,j}) d\psi_{i,j} = \sum_{j=1}^{4} \int \hat{n}(x,y) \cdot \vec{f}(x,y) dl \tag{31}$$

The order of the i and j sum in the second line has been interchanged. The i sum following the j sum in the beginning of the second line of Equation (31) has been converted to an integral on the right side of the second line in Equation (31). A uniform, positive length of each small rectangle, dl replaces $d\psi_{i,j}$, and the dependence of f on (x, y) anticipates the expression for $\vec{f}(x, y)$ in Equation (33). Integrating over i first leads to four terms in the second line of Equation (31), which constitute four line integrals to be used in the analysis in Equation (32). Note that interior rectangles in Figure 4 do not contribute to the line integrals because adjacent normals point in opposite directions. Therefore, only the external perimeter enclosed in dark blue lines in Figure 4 contributes to the second line of Equation (31), creating a macroscopic rectangle over which to integrate dot products as in Equation (32).

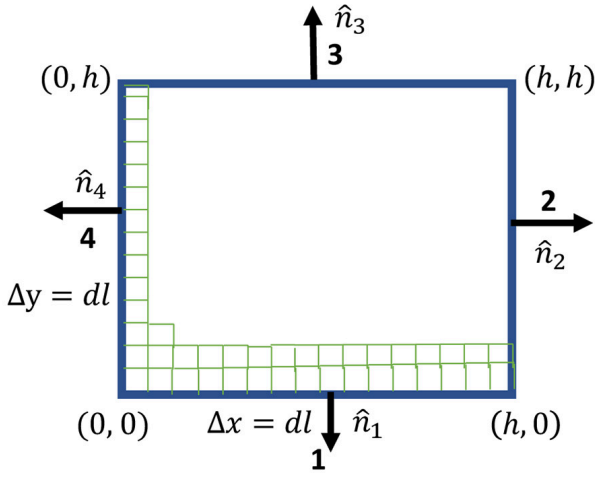

Figure 4. The macroscopic rectangle, with side lengths of h, is the path along which the line integral is taken of the function $\vec{f}$ dotted into the normals shown. This line integral along the four sides of the rectangle is shown to be equal to the two-dimensional divergence of $\vec{f}$ in Equation (31).

Expressing the normals in terms of rectangular coordinates (for example, $\hat{n}_1 = -\hat{y}$), and referring to Figure 4, the four integrals in the second line of Equation (31) become

$$\int_0^h \int_0^h D_\chi(Q) dx dy = \int_0^h (-\hat{y}) \cdot \vec{f}(l,0) dl + \int_0^h (\hat{x}) \cdot \vec{f}(h,l) dl + \int_0^h (\hat{y}) \cdot \vec{f}(l,h) dl - \int_0^h (\hat{x}) \cdot \vec{f}(0,l) dl, \tag{32}$$

where l is the path length of the outward sides of infinitesimal rectangles (in Figure 4).

B. Finding the Function $\vec{f}$ such that $\vec{\nabla}_2 \cdot \vec{f} = D_\chi$

In order to find a function $\vec{f}$ such that $\vec{\nabla}_2 \cdot \vec{f} = D_\chi(Q)$ as in Equation (31) and carry out the four 1D integrals in Equation (32), we follow the proposal in MF88 that $\vec{f}$ take

the form

$$\vec{f}(x,y) \quad = \quad (\vec{x}-\vec{\mu})G(Q) \tag{33}$$

with Q, $\vec{x}$, and $\vec{\mu}$ as in Equation (19) and where the correspondence between Γ, μ, Q_0, and the terms in Equation (18) is in Table 1. With $\vec{f}$ as in Equation (33), the two-dimensional divergence of $\vec{f}$ can be taken and set equal to $D_\chi(Q)$ to find $G(Q)$.

$$\begin{aligned} D_\chi(Q) = \vec{\nabla}_2 \cdot \vec{f}(x,y) &= \vec{\nabla}_2 \cdot (\vec{x}-\vec{\mu})G(Q) \\ &= \frac{df_x}{dx} + \frac{df_y}{dy} \\ &= 2G(Q) + (x-\mu_x)\frac{\partial G(Q)}{\partial x} + (y-\mu_y)\frac{\partial G(Q)}{\partial y} \\ &= 2G(Q) + 2\frac{\partial G(Q)}{\partial Q}(Q-Q_0) \\ &= 2\frac{\partial}{\partial Q}[(Q-Q_0)G(Q)] \end{aligned} \tag{34}$$

which is Equation (5) in MF88. In the third line of Equation (34), $\partial G(Q)/\partial x$ is calculated as $\frac{\partial G(Q)}{\partial Q}\frac{\partial Q}{\partial x}$, using Equation (20).

That Equation (34) is a simple derivative with respect to Q is the advantage of expressing the formulation in terms of a quadratic form. The expression for the divergence of $\vec{f}$ can be integrated to find $G(Q)$ in terms of $D_\chi(Q)$:

$$G(Q) = \frac{1}{2(Q-Q_0)}\int_{Q_0}^{Q} D_\chi(Q)dQ \tag{35}$$

From Equation (10), D_χ can be expressed in terms of $Q = R^2$:

$$D_\chi(R) = \frac{C^2R^{2/3}}{1+(\frac{R}{L})^{2/3}} = \frac{C^2Q^{1/3}}{1+(\frac{Q}{L^2})^{1/3}} = D_\chi(Q) \tag{36}$$

Following MF88, substituting Equation (36) into Equation (35) and setting $Q = L^2u^3$, $u = (Q/L^2)^{1/3}$, and $dQ = 3L^2u^2du$:

$$2(Q-Q_0)G(Q) = 3L^{8/3}C^2\int_{(\frac{Q_0}{L^2})^{1/3}}^{(\frac{Q}{L^2})^{1/3}} \frac{u^3}{1+u}du \tag{37}$$

The integral in Equation (37) can be done by dividing the denominator into the numerator, yielding

$$2(Q-Q_0)G(Q) = 3L^{8/3}C^2\int_{(\frac{Q_0}{L^2})^{1/3}}^{(\frac{Q}{L^2})^{1/3}} u^2-u+1-\frac{1}{1+u}du, \tag{38}$$

which yields an expression for $G(Q)$:

$$G(Q) = \frac{3L^{8/3}C^2}{2(Q-Q_0)}\left[\frac{u^3}{3}-\frac{u^2}{2}+u-\ln(1+u)\right]\Big|_{(\frac{Q_0}{L^2})^{1/3}}^{(\frac{Q}{L^2})^{1/3}}. \tag{39}$$

Having an expression for $G(Q)$, we can now formally substitute the expression for $\vec{f}$ of Equation (33) into the four lines of Equation (32):

$$\begin{aligned}\int_0^h \int_0^h D_\chi(Q)dxdy &= \int_0^h (-\hat{y}) \cdot (\vec{x} - \vec{\mu}) G(Q(l,0))dl + \int_0^h (\hat{x}) \cdot (\vec{x} - \vec{\mu}) G(Q(h,l))dl \\ &\quad + \int_0^h (\hat{y}) \cdot (\vec{x} - \vec{\mu}) G(Q(l,h))dl - \int_0^h (\hat{x}) \cdot (\vec{x} - \vec{\mu}) G(Q(0,l))dl \\ &= \int_0^h \mu_y G(Q(l,0))dl + \int_0^h (h - \mu_x) G(Q(h,l))dl \\ &\quad + \int_0^h (h - \mu_y) G(Q(l,h))dl + \int_0^h \mu_x G(Q(0,l))dl \end{aligned} \tag{40}$$

C. Summary of the Mathematical Formulation of the Tropospheric Covariance for VLBI Parameter Estimation

Tropospheric covariances are used 1) to evaluate the parameter estimate covariance due to tropospheric fluctuations (Equation [3]) and 2) to optimize the VLBI residual parameter estimates (Equation [6]). $\hat{P}_i$ are expressed in terms of tropospheric propagation delays in Equation (1). The tropospheric delay as a function of refractivity distribution, geometric paramters, and time is in Equation (7). The tropospheric covariance calculated from expressions of tropospheric delays is shown to depend on time-consuming double integrals of the refractivity structure function over the vertical path-length coordinate at each VLBI station, as in Equation (17).

Table 2 summarizes the calculational steps to perform four single integrals in place of the one double integral in Equation (17).

Table 2. Steps to perform four single integrals.

Step	Description	Equation/Location
1	Express geometric path-delay arguments of D_χ as a function of a quadratic form Q	(18)
2	Solve for Q parameters Γ, μ, and Q_0 in terms of parameters in Equation (18)	Table 1
3	Propose a candidate function, $\vec{f}$, the 2D divergence of which is D_χ	(33)
4	Take the divergence and solve for the key expression, $G(Q)$, in $\vec{f}$	(34), (35)
5	Express double integral over D_χ as four single integrals over $G(Q)$	(40)

VI. Future Studies to Assess Errors in the Use of the Covariance

The tropospheric covariance of Equation (3), via the various terms in Equation (17), involves parameters of wind speed and direction at each station. The wind vector may, in general, not be known to great accuracy. In order to assess the error introduced by having errors in the wind-vector terms, the tropospheric covariance matrix can be used to simulate tropospheric delays characterized by a range of wind vectors at each station. The simulation can be done by taking the square root of the covariance matrix and using it to transform white noise–simulated observations into observations with the tropospheric covariance [8].

The saturation scale should be tested in the same way, by generating tropospheric delays with a given saturation scale, and finding parameter covariances using saturation scales that differ from those in the simulated data.

Additional simulations of DSN-VLBI with non-parallel local verticals, and with a range of baseline lengths, will determine magnitude of the error in the covariance and consequent parameter estimates due to the flat-Earth assumption.

References

[1] J. B. Thomas, "An analysis of long baseline radio interferometry," NASA-JPL, Tech. Rep. 32-1526, vol. VII, pp. 37–50, 1972.

[2] R. N. Treuhaft and G. E. Lanyi, "The effect of the dynamic wet troposphere on radio interferometric measurements," *Radio Science*, vol. 22, no. 2, pp. 251–265, 1987.

[3] P. B. Liebelt, *An Introduction to Optimal Estimation*. Addison-Wesley Publishing, 1965.

[4] V. I. Tatarski, *Wave Propagation in a Turbulent Medium*. Dover Publications, 1961.

[5] W. C. Hamilton, *Statistics in Physical Science: Estimation, Hypothesis Testing, and Least Squares*. Ronald Press Co., 1964.

[6] E. Butkov, *Mathematical Physics*. Addison-Wesley Publishing, 1968.

[7] M. Finger, *Structure function integrals* Internal memo to R. Treuhaft, 1988.

[8] G. J. Bierman, *Factorization Methods for Discrete Sequential Estimation*. Academic Press, 1977.